PAPER

Impact of Antenna Correlation on Optimum Improved Energy Detector in Cognitive Radio

Sanket S. KALAMKAR[†a)], ***Student Member***, **Abhishek K. GUPTA**[††], ***Nonmember***, ***and*** **Adrish BANERJEE**[†b)], ***Member***

SUMMARY This paper investigates the detection performance of an improved energy detector for a secondary user with spatially correlated multiple antennas. In an improved energy detector, an arbitrary positive power operation p replaces the squaring operation in a conventional energy detector, and the optimum value of p that gives the best detection performance may be different from 2. Firstly, for a given value of p, we derive closed-form expressions for the probability of detection and the probability of false alarm when antennas at the secondary user are exponentially correlated. We then find the optimum value of p for two different detection criteria−maximizing the probability of detection for a target probability of false alarm, and minimizing the probability of false alarm for a target probability of detection. We show that the optimum p is strongly dependent on system parameters like number of antennas, antenna correlation coefficient among multiple antennas, and average received signal-to-noise ratio (SNR). From results, we infer that, in low SNR regime, the effect of antenna correlation is less pronounced on the optimum p. Finally, we find the optimum values of p and threshold jointly that minimize the total error rate.

key words: *cognitive radio; correlation, improved energy detector, multiple antennas, total error rate*

1. Introduction

Fixed allocation of the spectrum and its underutilization have led to spectrum scarcity [1]. Cognitive radio [2] is a promising solution that can overcome the problem of spectrum scarcity by allowing unlicensed or secondary users (SU) to opportunistically access the licensed or primary user (PU) bands. To access a PU band, SU needs to sense the presence of PU. If the PU band is found idle, SU may transmit over it. However, as soon as PU returns, SU must vacate the band to avoid harmful interference to PU. This process of sensing the PU occupancy is known as spectrum sensing [3].

Spectrum sensing is one of the most important components of cognitive radio. Accurate spectrum sensing is crucial to avoid miss detection and false detection of PU. Miss detection of PU may cause harmful interference to PU due to the secondary transmission over the band of interest. Thus, SU must be able to detect the primary transmissions even at low signal-to-noise ratio (SNR) satisfactorily with sufficiently high detection probability. On the other hand, due to false detection of PU, even if the incumbent of the spectrum is actually absent, SU would not be able to exploit the spectrum opportunities efficiently. Based on these requirements, we can measure the performance of a detection scheme in terms of two probabilities: the probability of detection and the probability of false alarm. The probability of detection is the probability of correctly detecting the presence of PU in the band; while, the probability of false alarm is the probability of falsely detecting the presence of PU in the band. For a good detection performance, the probability of detection should be as high as possible to avoid the harmful interference to PU and the probability of false alarm should be as low as possible to allow SU to exploit the spectrum usage opportunities efficiently. However, we cannot satisfy both conditions simultaneously, because the probability of false alarm increases with the probability of detection [4]. Thus, in practice, three criteria are used to evaluate the detection performance, which are as follows:

1. Maximization of the probability of detection keeping the probability of false alarm constant.
2. Minimization of the probability of false alarm keeping the probability of detection constant.
3. Minimization of the total error rate, that is, the sum of the probability of miss detection (1 − probability of detection) and the probability of false alarm. Minimizing the total error rate makes the detection scheme robust to sensing errors.

The first two criteria are also known as the Neyman-Pearson criteria [4].

Given the fact that the spectrum sensing lies at the heart of cognitive radio, a variety of spectrum sensing methods [5] like energy detection, matched filter detection [6], waveform-based sensing [7], and cyclostationary detection [3] have been proposed. Energy detection [8], [9] is a popular spectrum sensing method due to its easy implementation and low complexity. In conventional energy detection, the signal samples received by an SU are squared, summed, and then compared with a predetermined threshold to take a decision on the presence or absence of PU. However, energy detection suffers from an inferior detection performance at low SNR. In addition, multi-path fading, shadowing, and hidden terminal problem make PU detection more challenging[10]. To improve the detection performance of an energy detector, authors in [11] replace the squaring operation by an arbitrarily positive constant p, and then find the optimum value of p. This new energy detector is called *improved en-*

[†]The authors are with the Department of Electrical Engineering, Indian Institute of Technology Kanpur, Kanpur, India.

[††]The author is with the Department of Electrical and Computer Engineering, University of Texas at Austin, Austin, USA.

a) E-mail: kalamkar@iitk.ac.in

b) E-mail: adrish@iitk.ac.in

DOI: 10.1587/trans.E0.??.1

ergy detector, while the energy detector with squaring operation is called *conventional energy detector*. We can see that the improved energy detector with $p = 2$ is the conventional energy detector.

The key contributions of this paper are summarized as follows:

1. We derive closed-form expressions for the probabilities of detection and false alarm for an improved energy detector, when a secondary user is equipped with spatially correlated multiple antennas to sense the primary user.
2. We find the optimum value of power operation p for a given number of antennas and the correlation coefficient among them. We show that the optimum p changes with the correlation coefficient and number of antennas. Thus, to have the best detection performance, it is imperative to choose the power operation p according to the correlation coefficient and the number of antennas.
3. We study the effect of signal-to-noise ratio (SNR) on the optimum p, and show that the optimum p bears little effect of the correlation at low SNR regime. However, this optimum value of p might be different from $p = 2$, that is, from squaring operation in conventional energy detector.
4. To make sensing less prone to errors, it is necessary to minimize the total error rate. To achieve this, we jointly find the optimum value of p as well as the optimum threshold by simplifying the two variables problem to a single variable problem as presented in Sect. 4.3.

We organize the rest of the paper as follows. Section 2 highlights the related work, while Sect. 3 describes the system model. In Sect. 4, we perform the exact analysis of the improved energy detector for the antenna correlation. We also derive closed-form expressions of the probabilities of detection and false alarm. Further, we study the effect of correlation coefficient on the optimum p with low and high SNR approximations, and also find the optimum values of p and threshold jointly that minimize the total error rate. Section 5 provides the numerical results which show the effects of various system parameters like correlation coefficient, number of antennas, number of samples, and SNR on the optimum value of p for all the three performance criteria stated in Sect. 1. Finally, we draw the conclusions in Sect. 6.

2. Related Work

The works in [11]–[16] show that an improved energy detector can achieve the better detection performance than the conventional energy detector, that is, the optimum power operation p may be different from the squaring operation. In [17], [18], authors show that the value of $p \neq 2$ may provide more robustness against noise uncertainty in energy detection. For the improved energy detector, in [11]–[14], [17], [18], a single antenna is considered for spectrum sensing; whereas [19]–[23] use multiple antennas to improve the system performance of the conventional energy detection. In [24], authors have used multiple antennas for the improved energy detector and an optimum power operation p is found. However, in [24], the test statistic of the improved energy detector considers only a single sample of the received signal, while in general, multiple samples are required to achieve better performance. Also, the correlation among multiple antennas is not taken into consideration. In cognitive radio networks, the large distances between the sensing terminals and primary transmitter of SU cause small received channel angular spread value at the sensing terminals [25], making received signals at SU's antennas highly correlated. The effect of antenna correlation for the conventional energy detection is investigated in [25]–[29]. In [25], authors derive closed-form expressions for the probabilities of detection and false alarm under the conventional energy detection, when the sensing channels from the primary user to the secondary user's antennas are exponentially correlated and Rayleigh faded. In [26], authors derive a closed-form expression for the probability of detection with the conventional energy detection by employing square law combining when the sensing channels are correlated with Nakagami-m fading. In [27], authors propose a weighted energy detector to sense the presence or absence of the primary user over the exponentially correlated and Rayleigh faded sensing channels. In [28], the sub-optimum detectors based on the Rao test are proposed to determine the status of the primary users when the antennas at the secondary users are correlated, and when the correlation coefficient, PU signal power and noise variance are unknown. In [29], the trade-off between sensing efficiency and sensing accuracy for correlated antennas is shown. In [30], for the conventional energy detection, authors find the optimum threshold that minimizes the total error rate. To the best of our knowledge, this paper is the first work that studies the effect of correlation among multiple antennas on the performance of the improved energy detection.

3. System Model

We consider the system model similar to [11]. A binary hypothesis problem models the detection of PU as follows:

$$y_j = \begin{cases} s_j + n_j, & H_1, \\ n_j, & H_0, \end{cases} \tag{1}$$

where y_j is jth received sample by an antenna of an SU, s_j is jth sample of the block faded primary signal with $j = 1, 2, \ldots, N$, n_j is i.i.d. additive white Gaussian noise (AWGN) with zero mean and variance σ_n^2, H_1 and H_0 represent the hypotheses corresponding to the presence and absence of PU, respectively. s_j follows Gaussian distribution with zero mean and variance σ_s^2 [11]. We assume that the primary signal samples s_j are independent. The primary signal samples and noise samples are considered independent of each other.

Let M be the number of receive antennas at SU. We use the improved energy detection [11] for spectrum sensing. We can write the test statistic W for the improved energy

Table 1 Notation

Notation	Meaning
H_1	Hypothesis when the primary user is present
H_0	Hypothesis when the primary user is absent
M	Number of sensing antennas
N	Number of sensing samples
γ	Signal-to-noise ratio
p	An arbitrary positive power operation
ρ	Spatial correlation coefficient ($0 \le \rho \le 1$)
P_d	Probability of detection
P_f	Probability of false alarm
T	Sensing threshold at SU
p_{opt}	Optimum p
T_{opt}	Optimum threshold
σ_n^2	Noise variance at SU

detection as

$$W = \sum_{j=1}^{N} \sum_{i=1}^{M} \left(\left| \frac{y_{ij}}{\sigma_n} \right| \right)^p, \tag{2}$$

where y_{ij} is jth received sample by the ith antenna, $p > 0$ is an arbitrary constant. Using central limit theorem, for large N ($N > 10$), we may approximate W by Gaussian distribution [31]. We consider the exponential antenna correlation model:

3.1 Exponential Correlation Model

When antennas are equispaced in a linear fashion, the correlation among neighbouring antennas is higher than that of the distant antennas. In this case, the exponential antenna correlation model is more appropriate to describe the spatial correlation [25], [32], [33]. The exponential correlation model can be given in terms of antenna correlation matrix $\mathbf{R}^{\exp}_{M\times M}$ with its components $R^{\exp}_{mn}$ as

$$R^{\exp}_{mn} = \begin{cases} \rho^{n-m}, & m \le n, \\ R^{\exp}_{nm}, & m > n, \end{cases} \quad m, n = 1, \ldots, M. \tag{3}$$

4. Effect of Antenna Correlation on Detection Performance

Let

$$W_j = \sum_{i=1}^{M} \left(\left| \frac{y_{ij}}{\sigma_n} \right| \right)^p = \sum_{i=1}^{M} |Z_i|^p \tag{4}$$

for $j = 1, \ldots, N$, where $\dfrac{y_{ij}}{\sigma_n} = Z_i$. Here, the spatial correlation among antennas reflects in received samples y_{ij} on each antennas, which makes the test statistic W in Eq. (2) correlated. In the following subsections, we find the mean and variance of W under both hypotheses H_0 and H_1, and then derive the expressions for the probability of detection P_d and the probability of false alarm P_f.

4.1 Mean and Variance of W_j:

Let us define

$$G_p = \frac{2^{p/2}}{\sqrt{\pi}} \Gamma\left(\frac{p+1}{2} \right),$$

where $\Gamma(\cdot)$ is the ordinary gamma function. The mean of W_j can be given using [34, Eq. 3.462.9] as $\mu_{W_j} = \mathbb{E}[W_j] = M\mathbb{E}\left[\left| \dfrac{y_{ij}}{\sigma_n} \right|^p \right] = Mr^pG_p$ with

$$r = \frac{\sigma_y}{\sigma_n} = \begin{cases} 1, & H_0, \\ \sqrt{\gamma + 1}, & H_1, \end{cases} \tag{5}$$

where σ_y^2 is variance of the received signal y_{ij}, γ is average received signal-to-noise ratio (SNR) given by $\gamma = \dfrac{\sigma_s^2}{\sigma_n^2}$ and $\mathbb{E}[\cdot]$ is the expectation operator. Also, the variance of W_j can be given using [34, Eq. 3.462.9] as

$$\begin{aligned} \sigma^2_{W_j} &= \mathbb{E}[W_j^2] - (\mathbb{E}[W_j])^2 \\ &= \mathbb{E}\left[\left(\sum_{i=1}^{M} |Z_i|^p \right)^2 \right] - (Mr^pG_p)^2 \\ &= \mathbb{E}\left[\sum_{i=1}^{M} |Z_i|^{2p} + \sum_{m,n,m\neq n} |Z_m|^p |Z_n|^p \right] - (Mr^pG_p)^2 \\ &= r^{2p}(MG_{2p} - M^2G_p^2) + \sum_{m,n,m\neq n} \mathbb{E}\left[|Z_m|^p |Z_n|^p \right]. \end{aligned} \tag{6}$$

For exponential correlation model, we define c, related to the correlation between Z_m and Z_n, that is, the correlation between samples at mth and nth antenna, by Eq. (A· 3) as derived in the Appendix,

$$c = \frac{\mathbb{E}[Z_mZ_n]}{1+\gamma} = \frac{\gamma\rho^{|m-n|}}{1+\gamma}. \tag{7}$$

4.2 Mean and Variance of W:

We assume that at a given time, the received signal samples at different antennas may be correlated. Also, we consider the samples at an antenna are independent. Therefore, we can write mean μ_W and variance σ_W^2 of W as $\mu_W = \mathbb{E}[W] = N\mathbb{E}[W_j]$ and $\sigma_W^2 = N\sigma^2_{W_j}$, respectively.

Under H_0:

As the correlation coefficient ρ is zero, $\mathbf{R}$ becomes the identity matrix. So, Z_m and Z_n are independent. Also, from Eq. (5), $r = 1$. Then $\mathbb{E}[|Z_m|^p|Z_n|^p] = \mathbb{E}[|Z_m|^p]\mathbb{E}[|Z_n|^p] = G_p^2$ and the variance of W_j becomes

$$\begin{aligned} \sigma^2_{W_j} &= MG_{2p} - M^2G_p^2 + M(M-1)G_p^2 \\ &= M(G_{2p} - G_p^2). \end{aligned} \tag{8}$$

Therefore, we can write mean μ_0 and variance σ_0^2 of W under the hypothesis H_0 as $\mu_0 = MNG_p$ and $\sigma_0^2 = MN(G_{2p} - G_p^2)$, respectively.

Under H_1:

The mean μ_1 is given by

$$\mu_1 = N\mathbb{E}[W_j|H_1] = MNr^pG_p, \tag{9}$$

where r is $\sqrt{\gamma+1}$. The variance σ_1^2 of W is

$$\sigma_1^2 = N\left\{r^{2p}(MG_{2p} - M^2G_p^2) + \sum_{m,n,m\neq n}\mathbb{E}\left[|Z_m|^p|Z_n|^p\right]\right\}, \tag{10}$$

where $\mathbb{E}\left[|Z_m|^p|Z_n|^p\right]$ is given by

$$\begin{aligned}\mathbb{E}\left[|Z_m|^p|Z_n|^p\right] = \frac{r^{2p}}{\pi}\Gamma(p+1)(1-c^2)^{p+(1/2)}\mathcal{B}\left(\frac{1}{2}, p+1\right)\\ \times\left[F_1\left(p+1, p+1, \frac{1}{2}, p+\frac{3}{2}; c, -1\right)\right.\\ \left.+ F_1\left(p+1, p+1, \frac{1}{2}, p+\frac{3}{2}; -c, -1\right)\right],\end{aligned} \tag{11}$$

where $\mathcal{B}(\cdot,\cdot)$ is the beta function [34, 8.380] and F_1 is the hypergeometric function of two variables [34, 9.180]. The derivation of Eq. (11) is given in the Appendix.

Similar to H_0 case, for no correlation under H_1, Z_m and Z_n become independent. Then, the variance $\sigma^2_{1_{nc}}$ of W under H_1 can be given by a closed-form expression as

$$\sigma^2_{1_{nc}} = MN(1+\gamma)^p(G_{2p} - G_p^2). \tag{12}$$

The probability of detection P_d and the probability of false alarm P_f are given by $Pr(H_1|H_1)$ and $Pr(H_1|H_0)$, respectively. The probability of miss detection P_m is $1 - P_d$ and the total error rate P_t is given by $P_m + P_f$. From the test statistic given in Eq. (2) and using its Gaussian approximation, we can write the probability of detection as

$$P_d = \int_T^\infty \mathcal{N}(\mu_1, \sigma_1)\mathrm{d}x = Q\left(\frac{T-\mu_1}{\sigma_1}\right), \tag{13}$$

where T is the threshold, $\mathcal{N}(m, \sigma)$ represents Gaussian distribution with mean m and variance σ^2, $Q(\cdot)$ is given as $Q(t) = \frac{1}{\sqrt{2\pi}}\int_t^\infty \exp(-x^2/2)\mathrm{d}x$. μ_1 and σ_1 are given by Eq. (9) and Eq. (10), respectively. Similarly, we can write the probability of false alarm as

$$P_f = \int_T^\infty \mathcal{N}(\mu_0, \sigma_0)\mathrm{d}x = Q\left(\frac{T-\mu_0}{\sigma_0}\right), \tag{14}$$

where μ_0 and σ_0^2 denote mean and variance of W under H_0, respectively.

4.3 Joint Computation of Optimum p and Optimum Threshold

As shown in [11], the improved energy detector enhances the detection performance, by suitably choosing the power operation p. We will show in Sect. 5 that the optimum power operation p_{opt} may change with the correlation among multiple antennas. From Eq. (13) and Eq. (14), the expressions relating P_d and P_f independent of threshold T can be written as

$$P_d = Q\left(\frac{\sigma_0 Q^{-1}(P_f) + \mu_0 - \mu_1}{\sigma_1}\right), \tag{15}$$

$$P_f = Q\left(\frac{\sigma_1 Q^{-1}(P_d) + \mu_1 - \mu_0}{\sigma_0}\right). \tag{16}$$

We consider p_{opt} for three cases as follows:

1) p_{opt} that maximizes P_d for a fixed P_f: Numerical simulations are used to find p_{opt} using Eq. (15).
2) p_{opt} that minimizes P_f for a fixed P_d: Numerical simulations are used to find p_{opt} using Eq. (16).
3) p_{opt} along with the optimum threshold T_{opt} that minimizes the total error rate: Numerical simulations are used to find p_{opt} and T_{opt} using Eq. (17).

From Eq. (15) and Eq. (16), we can notice that for the first two criteria, finding p_{opt} is independent of the value of the threshold. However, third criterion, that is, the total error rate, depends on the value of p as well as the value of the threshold. Thus, to minimize the total error rate, the optimum value of p and the optimum value of threshold have to be computed jointly.

The total error rate P_t can be given by using Eq. (13) and Eq. (14) as

$$P_t = 1 - Q\left(\frac{T-\mu_1}{\sigma_1}\right) + Q\left(\frac{T-\mu_0}{\sigma_0}\right). \tag{17}$$

On differentiating Eq. (17) with respect to T for a fixed p, and equating to zero as

$$\frac{\partial P_t}{\partial T} = \frac{\exp\left(-\frac{1}{2}\left(\frac{T-\mu_1}{\sigma_1}\right)^2\right)}{\sigma_1} - \frac{\exp\left(-\frac{1}{2}\left(\frac{T-\mu_0}{\sigma_0}\right)^2\right)}{\sigma_0} = 0$$

yields the optimum threshold T_{opt}

$$T_{opt} = \frac{\mu_0\sigma_1^2 - \mu_1\sigma_0^2 + D\sigma_0\sigma_1}{\sigma_1^2 - \sigma_0^2}, \tag{18}$$

where $D = \sqrt{(\mu_1-\mu_0)^2 + 2(\sigma_1^2 - \sigma_0^2)\log_e(\sigma_1/\sigma_0)}$. It can be shown that the second derivative of P_t is positive at the optimum value of T. Substituting Eq. (18) in Eq. (17), p_{opt} can be obtained as follows:

$$\begin{aligned}p_{opt} = \arg\min_p \left\{1 - Q\left(\frac{(\mu_0-\mu_1)\sigma_1 + D\sigma_0}{\sigma_1^2 - \sigma_0^2}\right)\right.\\ \left.+Q\left(\frac{(\mu_0-\mu_1)\sigma_0 + D\sigma_1}{\sigma_1^2 - \sigma_0^2}\right)\right\}.\end{aligned} \tag{19}$$

From Eq. (19), we can see that the two variables problem of finding p_{opt} and T_{opt} is effectively reduced to a single

variable problem of finding p_{opt} only. The computation of Eq. (19) depends on Eq. (11) due to the presence of the term σ_1. Given the complex nature of Eq. (11), the optimum p, i.e., p_{opt} can be easily found numerically.

4.4 Low and high SNR Approximations

From Eq. (7), where $c = \dfrac{\gamma\rho^{|m-n|}}{1+\gamma}$, we can see that, for exponential correlation, c approaches 0 at low SNR, that is, the samples at different antennas tend to become uncorrelated. The system behaves as if it has independent multiple antennas even though the antennas are correlated. Thus, in low SNR regime, the effect of correlation among multiple antennas diminishes. From Eq. (10), Eq. (11), and Eq. (19), it can be shown that the optimum value of p becomes independent of c, and thus, of the correlation coefficient ρ.

At high SNR, it can be seen from Eq. (7) that c approaches $\rho^{|m-n|}$. Therefore, the correlation among multiple antennas affects the optimum value of p. The analysis is supported by the numerical results shown in Fig. 5.

5. Numerical Results

In this section, we present numerical results to show the effect of a number of antennas M, antenna correlation ρ, and average SNR on the optimum power operation p_{opt} that corresponds to following three criteria to measure the detection performance.

1. Maximization of P_d keeping P_f constant.
2. Minimization of P_f keeping P_d constant.
3. Minimization of the total error rate $P_m + P_f$.

The first two criteria are independent of the threshold T, and we only need to find the optimum p for given system parameters. In Fig. 1-6, we shall study the effect of aforementioned system parameters on the optimum p for the first two detection performance criteria. However, the third criterion is dependent on both p and threshold jointly. Thus, we need the optimum p and optimum threshold jointly that minimize the total error rate. In Fig. 7- 9, we shall numerically find the optimum pair of p and threshold jointly for given system parameters, and study the effects of them on the joint computation of p_{opt} and T_{opt}. The system parameters considered are given along with respective figures.

5.1 Effect of p on the detection performance

Figure 1 shows P_d versus p for a fixed P_f with three correlated multiple antennas. The correlation coefficient ρ is set to 0.5. We can see that there exists an optimum value p_{opt} of $p \neq 2$ that maximizes P_d for a given P_f. Also, p_{opt} that maximizes P_d changes with P_f; in particular, as the target P_f decreases, making constraint more stringent, p_{opt} that maximizes P_d increases. Also, note that the maximum value of P_d achieved falls as the target P_f is set to a lower value. Similarly, p_{opt} that minimizes P_f for a fixed

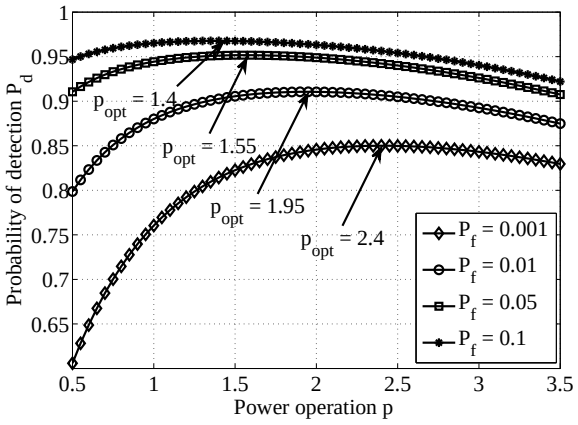

Fig. 1 P_d versus p for different probability of false alarm P_f, $\rho = 0.5$, $M = 3$, $N = 20$, $\sigma_n^2 = 1$, SNR = 0 dB.

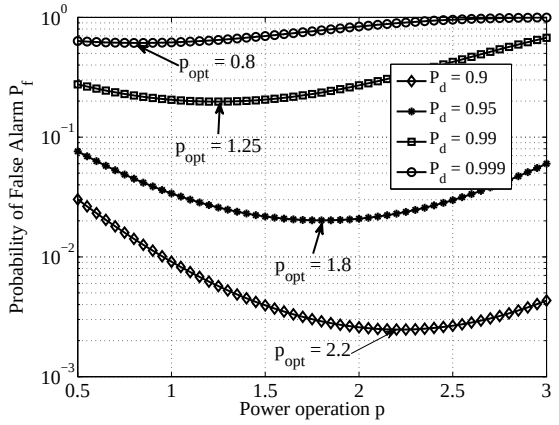

Fig. 2 P_f versus p for different probability of detection P_d, $\rho = 0.5$, $M = 3$, $N = 20$, $\sigma_n^2 = 1$, SNR = 0 dB.

P_d can be obtained, and is shown in Fig. 2. Here, as the target P_d increases, making constraint more stringent, p_{opt} that minimizes P_f reduces, while the minimum value of P_f that can be obtained increases.

5.2 Effect of the correlation coefficient on the optimum p

Figure 3 and 4 show the variation of p_{opt} with antenna correlation coefficient ρ for different number of antennas M. In Fig. 3, for a fixed P_d, p_{opt} is calculated that minimizes P_f. As the correlation among antennas increases, p_{opt} that minimizes P_f decreases. Figure 4 shows the variation of p_{opt} against ρ that maximizes P_d when P_f is fixed to 0.01. It can also be noticed from Fig. 3 and 4 that for the case of maximizing P_d while keeping P_f constant, the optimum value of p remains almost the same irrespective of the correlation coefficient for a given number of antennas; while the optimum p changes significantly with the correlation coefficient when we try to minimize P_f for a given P_d.

Figure 5 and 6 show the effect of average received SNR

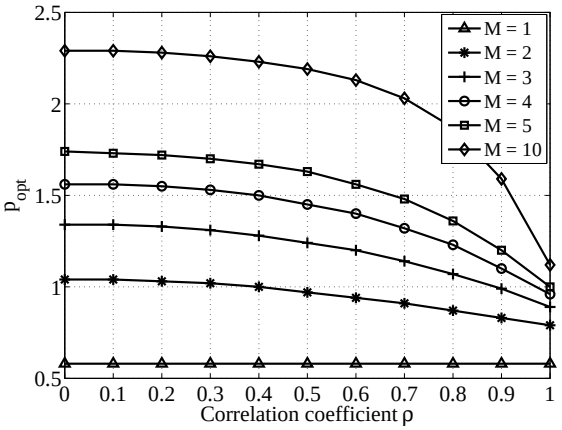

Fig. 3 p_{opt} versus ρ. Minimizing P_f for a fixed P_d for multiple antennas M, $P_d = 0.99$, $N = 20$, $\sigma_n^2 = 1$, SNR = 0 dB. For $M = 1$, the correlation is not applicable and p_{opt} remains constant.

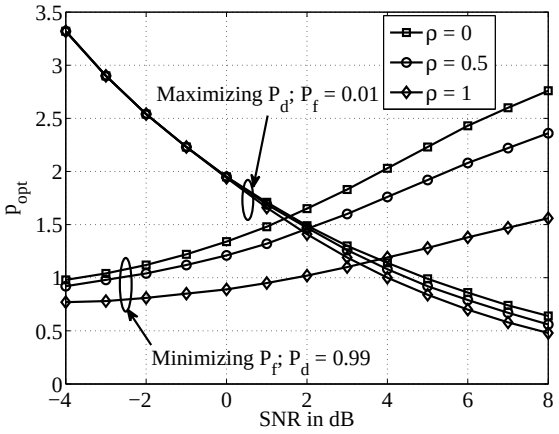

Fig. 5 Optimum value of p, maximizing P_d against SNR for different values of ρ for a fixed P_f and M, as well as optimum value of p, minimizing P_f against SNR for different values of ρ for a fixed P_d, $M = 3$, $N = 20$.

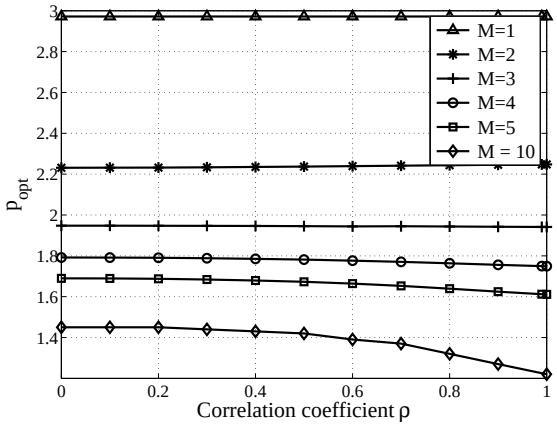

Fig. 4 Exponential correlation: p_{opt} versus ρ. Maximizing P_d for a fixed P_f for multiple antennas M, $P_f = 0.01$, $N = 20$, $\sigma_n^2 = 1$, SNR = 0 dB. For $M = 1$, the correlation is not applicable and p_{opt} remains constant.

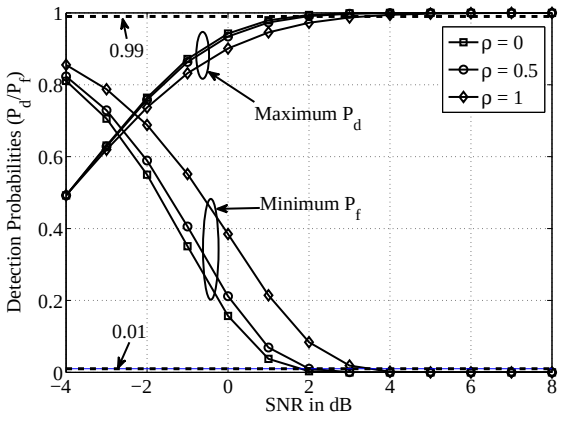

Fig. 6 Maximized P_d and minimized P_f corresponding to the optimum value of p in Fig. 5 versus SNR for different values of ρ, $M = 3$, $N = 20$.

on p_{opt}, and corresponding maximized P_d and minimized P_f, respectively, for different ρ and $M = 3$. As discussed in Sect. 4.4, at low SNR, the antennas become almost independent and ρ has no effect on p_{opt}. This can be seen in Fig. 5, where the curves corresponding to $\rho = 0$, 0.5, 1 approach each other in low SNR regime. At high SNR, c approaches $\rho^{|m-n|}$, thus ρ affects p_{opt}. This is evident in Fig. 5, where at high SNR values, the curves corresponding to $\rho = 0$, 0.5, 1 start diverging from each other. Now, let us pay special attention to the SNR value that corresponds to the intersection of curves for "Maximizing P_d when target $P_f = 0.01$" and "Minimizing P_f when target $P_d = 0.99$" in Fig. 5 for a given ρ. We note that, for a given ρ, the point of intersection gives the values of p_{opt} and SNR for which $P_d = 0.99$ and $P_f = 0.01$ at the same time. For example, if we look at both curves for $\rho = 0.5$, we can notice that p_{opt} and SNR at the intersection of curves are 1.47 and 2 dB, respectively, i.e., to achieve $P_d = 0.99$ and $P_f = 0.01$ for $\rho = 0.5$, one should choose p to be 1.47, and the required SNR is 2 dB. Now, for $\rho = 0$, we can see from Fig. 5 that, at the point of intersection, $p_{opt} = 1.57$ and SNR = 1.6 dB; while for $\rho = 1$, $p_{opt} = 1.12$ and SNR = 3.35 dB. From aforementioned observations, we remark that, with the increase in ρ, the required SNR to obtain $P_d = 0.99$ and $P_f = 0.01$ increases, while corresponding p_{opt} decreases.

The above discussion can also be validated from Fig. 6, which plots "Maximum P_d" and "Minimum P_f" corresponding to p_{opt} in Fig. 5 for given ρ and SNR. For example, consider the case when $\rho = 0.5$. In this case, the intersection of the curve for "Maximum P_d" with the dashed line of '0.99' and the intersection of the curve for "Minimum P_f" with the dashed line of '0.01' occur simultaneously at SNR = 2 dB, which is same as the one obtained from Fig. 5. We also confirm from Fig. 6 that, the required SNR to satisfy $P_d = 0.99$ and $P_f = 0.01$ simultaneously increases with increase in ρ.

From Fig. 1-6, one can conclude that p_{opt} depends on

system parameters like target P_d, target P_f, SNR, M, and ρ. Thus, p_{opt} in an improved energy detector can be determined according to given system parameters, along with the graphs shown in Fig. 1-6.

5.3 Minimizing the total error rate

Let us now look at the minimization of the total error rate P_t. Here, we aim to minimize the overall sensing errors, i.e., $P_m + P_f$, instead of just minimizing only one of the sensing errors (P_m or P_f) keeping other sensing error fixed. Unlike the minimization of only one sensing error (Fig. 3-6) which requires finding only optimum p for given system parameters, from Eq. (13), Eq. (14), and Eq. (17), we can see that the minimization of the total error rate P_t is dependent on both p and threshold T. That is, to obtain the minimum total error rate, we have to find corresponding optimum p and T jointly, as discussed in Sect. 4.3.

Figure 7 shows the joint effect of p and threshold T on the total error rate, where we can see that there exists an optimum pair of p and T that minimizes the total error rate. Figure 8 shows the jointly found optimum values of p and threshold that minimize P_t for different number of antennas, against the correlation coefficient ρ; while Fig. 9 plots the corresponding values of minimized total error rate. For example, when $\rho = 0.5$ and $M = 3$, the optimum pair (p_{opt}, T_{opt}) that minimizes P_t is found to be (1.78, 74.4), and the corresponding minimized P_t is 0.07. From Fig. 8, note that increase in ρ decreases the optimum p as well as the optimum threshold. This trend of the optimum p that minimizes $P_t = P_m + P_f$ is expected as both the optimum p that maximizes P_d (in turn, minimizes P_m) and the optimum p that minimizes P_f, decrease with the increase in ρ (please see Fig. 3 and 4). Also, from Fig. 9, we can observe the deteriorating effect of correlation, i.e., higher correlation among antennas leads to the increase in the minimized total error rate. This is expected as the antenna correlation reduces the degrees of freedom. On the other hand, increase in the number of antennas M improves the detection performance due to the increased spatial diversity, in turn, obtaining lower minimum P_t for a given correlation coefficient.

Figure 8 provides guidelines to select p and threshold jointly to minimize the total error rate for given system parameters, so that the opportunity to use the idle spectrum improves (by minimizing the probability of false alarm) while keeping the interference to the primary user below the given limit (by maximizing the probability of detection); Fig. 9 allows us to decide whether the minimized total error rate is acceptable in practice.

6. Conclusions

The optimum power operation p_{opt} for the improved energy detector changes with the number of antennas M, correlation coefficient ρ among multiple antennas, number of samples and average received SNR, and may be different from $p = 2$ (conventional energy detection). Thus, the value of p should be chosen according to above system parameters. Moreover, we note that maximizing the probability of detection for a given probability of false alarm is more robust to the effect of correlation among multiple antennas than minimizing the probability of false alarm for a given probability

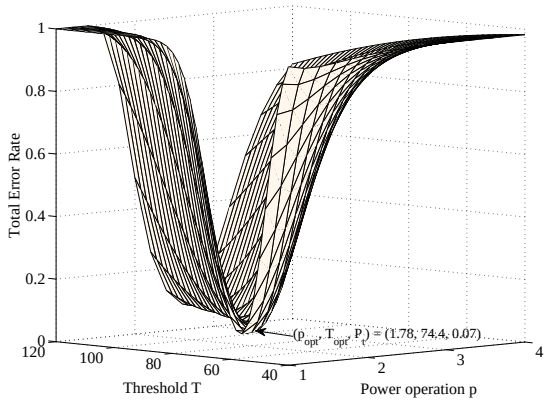

Fig. 7 Total error rate against the threshold T and the power operation p, $\rho = 0.5$, $M = 3$, SNR = 0 dB, $N = 20$.

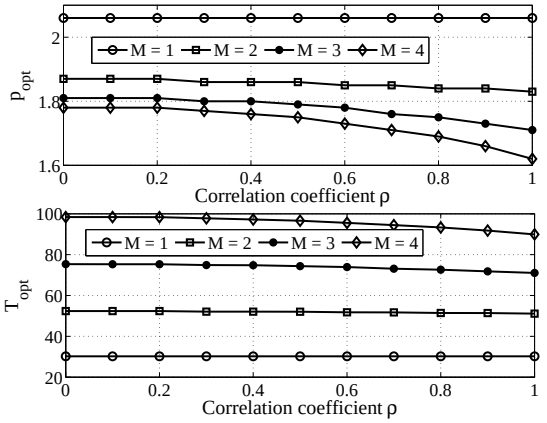

Fig. 8 Finding p_{opt} and T_{opt} jointly, minimizing $P_t = P_m + P_f$ against different ρ and M, $N = 20$, SNR = 0 dB. For $M = 1$, the correlation is not applicable and p_{opt} remains constant.

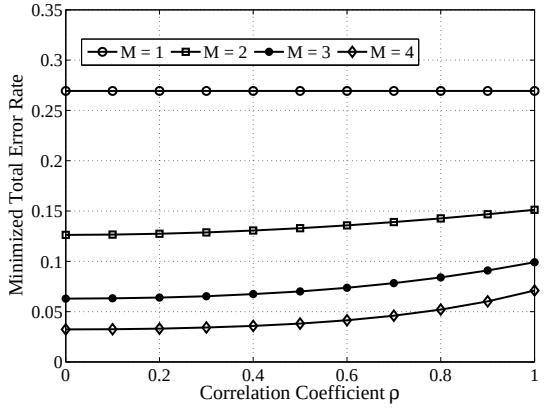

Fig. 9 Minimized total error rate versus the correlation coefficient ρ and number of antennas M, $N = 20$, SNR = 0 dB. For $M = 1$, the correlation is not applicable, and the minimized total error rate remains constant.

of detection; while for minimization of total error rate, the optimum p and threshold are only affected by high correlation values. Numerical results show that in low SNR regime, the effect of correlation on p_{opt} diminishes. We also calculate the optimum pair of p_{opt} and threshold jointly to minimize the total error rate, and show that the optimum pair may change with ρ and M.

Acknowledgments

This work is supported in part by a research grant from the Indo-UK Advanced Technology Centre. Sanket S. Kalamkar is supported by the Tata Consultancy Services (TCS) research fellowship.

References

[1] FCC, "Spectrum policy task force," ET Docket 02-135, Nov. 2002.
[2] J. Mitola and G. Maguire, "Cognitive radio: Making software more personal," IEEE Pers. Commun., vol.6, pp.13–18, Aug. 1999.
[3] T. Yucek and H. Arslan, "A survey of spectrum sensing algorithms for cognitive radio applications," IEEE Commun. Surveys and Tutorials, vol.11, no.1, pp.116–130, 2009.
[4] S. Kay, Fundamentals of Statistical Signal Processing, Volume II: Detection Theory, Prentice Hall, 1998.
[5] E. Axell, G. Leus, E. Larsson, and H. Poor, "Spectrum sensing for cognitive radio : State-of-the-Art and recent advances," IEEE Signal Process. Mag., vol.29, no.3, pp.101–116, 2012.
[6] R. Tandra and A. Sahai, "Fundamental limits on detection in low SNR under noise uncertainty," Proc. Int. Conf. on Wireless Networks, Commun. and Mobile Computing, pp.464–469, June 2005.
[7] H. Tang, "Some physical layer issues of wide-band cognitive radio systems," Proc. IEEE Int. Symp. on New Frontiers in Dynamic Spectrum Access Networks, pp.151–159, Nov. 2005.
[8] H. Urkowitz, "Energy detection of unknown deterministic signals," Proc. IEEE, vol.55, no.4, pp.523–531, April 1967.
[9] F. Digham, M. Alouini, and M. Simon, "On the energy detection of unknown signals over fading channels," IEEE Trans. Commun., vol.55, no.1, pp.21–14, Jan. 2007.
[10] A. Ghasemi and E. Sousa, "Collaborative spectrum sensing for opportunistic access in fading environments," Proc. IEEE Int. Symp. on New Frontiers in Dynamic Spectrum Access Networks, pp.131–136, Nov. 2005.
[11] Y. Chen, "Improved energy detector for random signals in Gaussian noise," IEEE Trans. Wireless Commun., vol.9, no.2, pp.558–563, Feb. 2010.
[12] J. Song, Z. Feng, P. Zhang, and Z. Liu, "Spectrum sensing in cognitive radios based on enhanced energy detector," IET Commun., vol.6, no.8, pp.805–809, May 2012.
[13] V. Sharma Banjade, C. Tellambura, and H. Jiang, "Performance of p-norm detector in AWGN, fading and diversity reception," IEEE Trans. Veh. Technol., vol.63, no.7, pp.3209–3222, Sept. 2014.
[14] A. Singh, M.R. Bhatnagar, and R.K. Mallik, "Performance analysis of multiple sample based improved energy detector in collaborative CR networks," Proc. IEEE Int. Symp. on Person. Indoor and Mobile Radio Commun., pp.2728–2732, Sept. 2013.
[15] S. Kalamkar and A. Banerjee, "Improved double threshold energy detection for cooperative spectrum sensing in cognitive radio," Defence Science Journal (Special Issue on Communication Systems and Image Processing Technologies), vol.63, no.1, pp.34–40, Jan. 2013.
[16] S. Nallagonda, A. Chandra, S.D. Roy, and S. Kundu, "Performance of improved energy detector based cooperative spectrum sensing over Hoyt and Rician faded channels," IEICE Commun. Express, vol.2, no.7, pp.319–324, 2013.
[17] S. Kalamkar and A. Banerjee, "On the performance of generalized energy detector under noise uncertainty in cognitive radio," Proc. National Conf. on Commun., pp.1–5, Feb. 2013.
[18] S. Kalamkar, A. Banerjee, and A.K. Gupta, "SNR wall for generalized energy detection under noise uncertainty in cognitive radio," Proc. Asia-Pacific Conf. on Commun., pp.375–380, Aug. 2013.
[19] A. Pandharipande and J. Linnartz, "Performance analysis of primary user detection in a multiple antenna cognitive radio," Proc. IEEE Int. Conf. on Commun., pp.6482–6486, 2007.
[20] A. Taherpour, M. Nasiri-Kenari, and S. Gazor, "Multiple antenna spectrum sensing in cognitive radios," IEEE Trans. Wireless Commun., vol.9, no.2, pp.814–823, Feb. 2010.
[21] R. Zhang, T.J. Lim, Y.C. Liang, and Y. Zeng, "Multi-antenna based spectrum sensing for cognitive radios: A GLRT approach," IEEE Trans. Commun., vol.58, no.1, pp.84–88, 2010.
[22] M. Alamgir, M. Faulkner, J. Gao, and P. Conder, "Signal detection for cognitive radio using multiple antennas," Proc. Int. Symp. on Wireless Commun. Systems, pp.488–492, 2008.
[23] K. Umebayashi, H. Tsuchiya, and Y. Suzuki, "Analysis of optimal weighted cooperative spectrum sensing with multiple antenna elements," IEICE Trans. Commun., vol.E95.B, no.10, pp.3261–3269, 2012.
[24] A. Singh, M. Bhatnagar, and R. Mallik, "Cooperative spectrum sensing in multiple antenna based cognitive radio network using an improved energy detector," IEEE Commun. Lett., vol.16, no.1, pp.64–67, Jan. 2012.
[25] S. Kim, J. Lee, H. Wang, and D. Hong, "Sensing performance of energy detector with correlated multiple antennas," IEEE Signal Process. Lett., vol.16, no.8, pp.671–674, Aug. 2009.
[26] V. Banjade, N. Rajatheva, and C. Tellambura, "Performance analysis of energy detection with multiple correlated antenna cognitive radio in Nakagami-m fading," IEEE Commun. Lett., vol.16, no.4, pp.502–505, April 2012.
[27] L. Luo, P. Zhang, G. Zhang, and J. Qin, "Spectrum sensing for cognitive radio networks with correlated multiple antennas," Electron. Lett., vol.47, no.23, pp.1297–1298, Oct. 2011.
[28] S. Sedighi, A. Taherpour, and J. Sala, "Spectrum sensing using correlated receiving multiple antennas in cognitive radios," IEEE Trans. Wireless Commun., vol.12, no.11, pp.5754–5766, 2013.
[29] Y. Liu, Y. Wang, and G. Wei, "Performance improvement in cognitive radio systems with correlated multiple antennas," IEICE Trans. Commun., vol.E94-B, no.4, pp.1053–1056, April 2011.
[30] W. Zhang, R. Mallik, and K. Letaief, "Optimization of cooperative spectrum sensing with energy detection in cognitive radio networks," IEEE Trans. Wireless Commun., vol.8, no.12, pp.5761–5766, Dec. 2009.
[31] A. Papoulis and S. Pillai, Probability, Random Variables and Stochastic Processes, 4th ed., McGraw Hill, 2002.
[32] V. Aalo, "Performance of maximal-ratio diversity systems in a correlated Nakagami-fading environment," IEEE Trans. Commun., vol.43, no.8, pp.2360–2369, 1995.
[33] S. Loyka, "Channel capacity of MIMO architecture using exponential correlation matrix," IEEE Commun. Lett., vol.5, pp.369–371, Sep. 2001.
[34] I. Gradshteyn and I. Ryzhik, Table of Integrals, Series and Products, 6th ed., Academic Press, 2000.

Appendix: Proof of Eq. (11)

Let I be defined as

$$I = \mathbb{E}\left[|Z_m|^p |Z_m|^p\right] = \int_0^\infty \int_0^\infty |z_m|^p |z_n|^p f(z_m, z_n) \mathrm{d}z_m \mathrm{d}z_n, \quad (\mathrm{A}\cdot 1)$$

where $f(z_m, z_n)$ is the joint probability density function of Z_m and Z_n. $\mathbf{Z}_{mn} = [Z_m\ Z_n]$ is a bivariate distribution with mean $\mathbf{M} = [0\ \ 0]$ and covariance matrix

$$\mathbf{V} = \begin{bmatrix} r^2 & \gamma\rho^{|m-n|} \\ \gamma\rho^{|m-n|} & r^2 \end{bmatrix} = \begin{bmatrix} r^2 & cr^2 \\ cr^2 & r^2 \end{bmatrix}, \quad (\text{A}\cdot 2)$$

where r is $\sqrt{1+\gamma}$ under H_1, and c is given by

$$c = \frac{\gamma\rho^{|m-n|}}{1+\gamma}. \quad (\text{A}\cdot 3)$$

So $f(z_m, z_n)$ can be written as

$$f(z_m, z_n) = \frac{1}{2\pi r^2\sqrt{1-c^2}} \times \exp\left(-\frac{1}{2}\frac{1}{1-c^2}\left(\frac{z_m^2}{r^2} - 2c\frac{z_m z_n}{r^2} + \frac{z_n^2}{r^2}\right)\right). \quad (\text{A}\cdot 4)$$

Thus, the integration I to be solved, is obtained by substituting Eq. (A· 4) in Eq. (A· 1). By using transformation of random variables, $U = \frac{Z_m}{r}$ and $V = \frac{Z_n}{r}$, we can write Eq. (A· 1) as

$$I = \frac{1}{2\pi\sqrt{1-c^2}} r^{2p} \int_0^\infty \int_0^\infty |u|^p |v|^p \times \exp\left(-\frac{1}{2}\frac{1}{1-c^2}\left(u^2 - 2cuv + v^2\right)\right) \mathrm{d}u\ \mathrm{d}v. \quad (\text{A}\cdot 5)$$

We again make use of transformation of random variables, $U = A\cos t$ and $V = A\sin t$. Then, we can write Eq. (A· 5) as

$$I = \frac{1}{2^p}\frac{r^{2p}}{2\pi\sqrt{1-c^2}} \int_0^{2\pi} |\sin 2t|^p \int_0^\infty |a|^{2p+1} \times \exp\left(-\frac{1}{2}\frac{a^2}{1-c^2}(1 - c\sin 2t)\right) \mathrm{d}a\ \mathrm{d}t. \quad (\text{A}\cdot 6)$$

We first solve inner integral I_1 given as

$$I_1 = \int_0^\infty |a|^{2p+1} \exp\left(-\frac{1}{2}\frac{a^2}{1-c^2}(1 - c\sin 2t)\right) \mathrm{d}a. \quad (\text{A}\cdot 7)$$

Let $k = \frac{1}{2}\frac{1}{1-c^2}(1 - c\sin 2t)$. Substituting $ka^2 = w$, the inner integral I_1 becomes

$$I_1 = \frac{1}{2k}\int_0^\infty \left|\frac{w}{k}\right|^p \exp(-w)\mathrm{d}w = 2^p\Gamma(p+1)\left(\frac{1-c^2}{(1-c\sin 2t)}\right)^{p+1}. \quad (\text{A}\cdot 8)$$

Substituting Eq. (A· 8) in Eq. (A· 6) and simplifying further, we get

$$I = \frac{1}{2\pi} r^{2p}\Gamma(p+1)(1-c^2)^{p+(1/2)} \int_0^{2\pi} \frac{|\sin t|^p}{(1-c\sin t)^{p+1}}\mathrm{d}t. \quad (\text{A}\cdot 9)$$

Now, the integral I_2 to be solved is as follows:

$$I_2 = \int_0^{2\pi} \frac{|\sin t|^p}{(1-c\sin t)^{p+1}}\mathrm{d}t. \quad (\text{A}\cdot 10)$$

Then, we can write Eq. (A· 10) as

$$I_2 = 2\int_0^{\pi/2} \frac{(\sin t)^p}{(1-c\sin t)^{p+1}}\mathrm{d}t + 2\int_\pi^{3\pi/2} \frac{(-\sin t)^p}{(1-c\sin t)^{p+1}}\mathrm{d}t. \quad (\text{A}\cdot 11)$$

Putting $-\sin t = x$ in Eq. (A· 11), we have

$$I_2 = 2\int_0^1 \frac{x^p}{(1-cx)^{p+1}\sqrt{1-x^2}}\mathrm{d}x + 2\int_0^1 \frac{x^p}{(1+cx)^{p+1}\sqrt{1-x^2}}\mathrm{d}x. \quad (\text{A}\cdot 12)$$

Let the first integral of Eq. (A· 12) be

$$I_3 = \int_0^1 x^p(1-cx)^{-(p+1)}(1-x^2)^{-1/2}\mathrm{d}x, \quad (\text{A}\cdot 13)$$

and the second integral of Eq. (A· 12) be

$$I_4 = \int_0^1 x^p(1+cx)^{-(p+1)}(1-x^2)^{-1/2}\mathrm{d}x. \quad (\text{A}\cdot 14)$$

Using [34, 3.211], we can write I_3 and I_4 in (A· 13) and (A· 14) as

$$I_3 = \mathcal{B}\left(\frac{1}{2}, p+1\right) F_1\left(p+1, p+1, \frac{1}{2}, p+\frac{3}{2}; c, -1\right) \quad (\text{A}\cdot 15)$$

and

$$I_4 = \mathcal{B}\left(\frac{1}{2}, p+1\right) F_1\left(p+1, p+1, \frac{1}{2}, p+\frac{3}{2}; -c, -1\right), \quad (\text{A}\cdot 16)$$

respectively, where $\mathcal{B}(\cdot,\cdot)$ is the beta function (please see [34, 8.380]) and F_1 is the hypergeometric function of two variables (please see [34, 9.180]). Then, we can write I_2 in (A· 12) as

$$I_2 = 2\mathcal{B}\left(\frac{1}{2}, p+1\right)\left[F_1\left(p+1, p+1, \frac{1}{2}, p+\frac{3}{2}; c, -1\right) + F_1\left(p+1, p+1, \frac{1}{2}, p+\frac{3}{2}; -c, -1\right)\right]. \quad (\text{A}\cdot 17)$$

Substituting I_2 from (A· 17) in (A· 9), we can write Eq. (11) as follows:

$$I = \frac{1}{\pi} r^{2p} \Gamma(p+1)(1-c^2)^{p+(1/2)} \mathcal{B}\left(\frac{1}{2}, p+1\right) \times \left[F_1\left(p+1, p+1, \frac{1}{2}, p+\frac{3}{2}; c, -1\right) + F_1\left(p+1, p+1, \frac{1}{2}, p+\frac{3}{2}; -c, -1\right)\right]. \quad (A \cdot 18)$$

Sanket S. Kalamkar received his BTech from College of Engineering Pune, Pune, India, in 2009. He is presently working towards his PhD at the Department of Electrical Engineering, Indian Institute of Technology Kanpur, Kanpur, India. His research interests include: cognitive radio networks, wireless communications, and coding theory. He is a recipient of Tata Consultancy Services (TCS) research scholarship.

Abhishek K. Gupta received his BTech and MTech in Electrical Engineering from Indian Institute of Technology Kanpur, Kanpur, India, in 2010. He is currently a PhD student at The University of Texas at Austin, where his research has focused on stochastic geometry and its applications in wireless communication. His other research interests include multiuser MIMO systems and optimization. He was recipient of GE-FS Leadership Award by General Electric (GE) Foundation and Institute of International Education in 2009.

Adrish Banerjee received his BTech from Indian Institute of Technology, Kharagpur, India, and MS and PhD from University of Notre Dame, Indiana. He is currently an Associate Professor in the Department of Electrical Engineering at Indian Institute of Technology, Kanpur. His research interests include: physical layer aspects of wireless communications, particularly error control coding, cognitive radio, and green communications.